ADVANCED MATERIALS INTERFACES
www.advmatinterfaces.de

Characterizing Electron Flow through Catechol-Graphene Composite Hydrogels

*Eunkyoung Kim, Rita Argenziano, Zhiling Zhao, Chen-yu Chen, Margaret Shen, William E. Bentley, Alessandra Napolitano, and Gregory F. Payne**

Electronic materials that allow the controlled flow of electrons in aqueous media are required for emerging applications that require biocompatibility, safety, and/or sustainability. Here, a composite hydrogel film composed of graphene and catechol is electrofabricated, and that this composite offers synergistic properties is reported. Graphene confers metal-like conductivity and enables charge-storage through an electrical double layer mechanism. Catechol confers redox-activity and enables charge-storage through a redox mechanism. Importantly, there are two functional populations of catechols: conducting-catechols (presumably in intimate contact with graphene) allow direct electron-transfer; and non-conducting-catechols (presumably physically separated from graphene) require diffusible mediators to enable electron-transfer. Using a variety of spectroelectrochemical measurements, that the capacity of the composite for charge-storage increases in proportion to the extent by which the catechol-groups can undergo redox-state switching is demonstrated. To illustrate the broad relevance of this work, how the redox-state switching can be related to both the charge storage of energy materials and the memory of molecular electronic materials is discussed. The authors believe this work is significant because it demonstrates that: conducting and redox-active components enable distinctly different mechanisms for charge-storage and electron-transfer; these components act synergistically; and mediators provide unique opportunities to extend the capabilities of electronic materials.

1. Introduction

The creation of improved electronic materials relies on understanding the mechanisms responsible for charge-storage and electron-transfer, and then controlling these mechanisms for user-defined purposes. For energy applications (e.g., capacitors and batteries), the focus is on storing large quantities of electrons and controlling their discharge.[1–3] For information processing applications (e.g., electronics),[4,5] materials are desired that can gate and rectify electron-flow.[6,7] Other applications focus on materials that offer state-dependent properties (e.g., optoelectronics)[8] or memory (e.g., memristors).[9] With the growing emphasis on safety and sustainability, and the expanding interest in life-science applications, there is an increasing interest in the development of electronic materials that function in aqueous systems.[10]

In aqueous systems, electron-transfer is constrained by the solvent and typically occurs through at least two distinctly different mechanisms each of which favors different types of materials.[11–13] One electron-transfer mechanism is a metal-like conductivity.[14,15] Carbon-based nanomaterials have been especially important for conferring such conductivity[14,16] with benefits that include enhanced double layer charge storage for energy applications[17–21] and electrocatalytic properties for sensing applications.[22–24] A second electron-transfer mechanism involves reduction–oxidation (redox) reactions. Redox polymers offer such properties and have been used in applications that include energy

E. Kim, Z. Zhao, M. Shen, W. E. Bentley, G. F. Payne
Institute for Bioscience and Biotechnology Research
University of Maryland
College Park, MD 20742, USA
E-mail: gpayne@umd.edu

The ORCID identification number(s) for the author(s) of this article can be found under https://doi.org/10.1002/admi.202202021.

DOI: 10.1002/admi.202202021

E. Kim, Z. Zhao, W. E. Bentley, G. F. Payne
Robert E. Fischell Institute for Biomedical Devices
University of Maryland
College Park, MD 20742, USA

R. Argenziano, A. Napolitano
Department of Chemical Sciences
University of Naples Federico II
Via Cintia 4, Naples I-80126, Italy

C.-y. Chen, W. E. Bentley
Fischell Department of Bioengineering
University of Maryland
College Park, MD 20742, USA

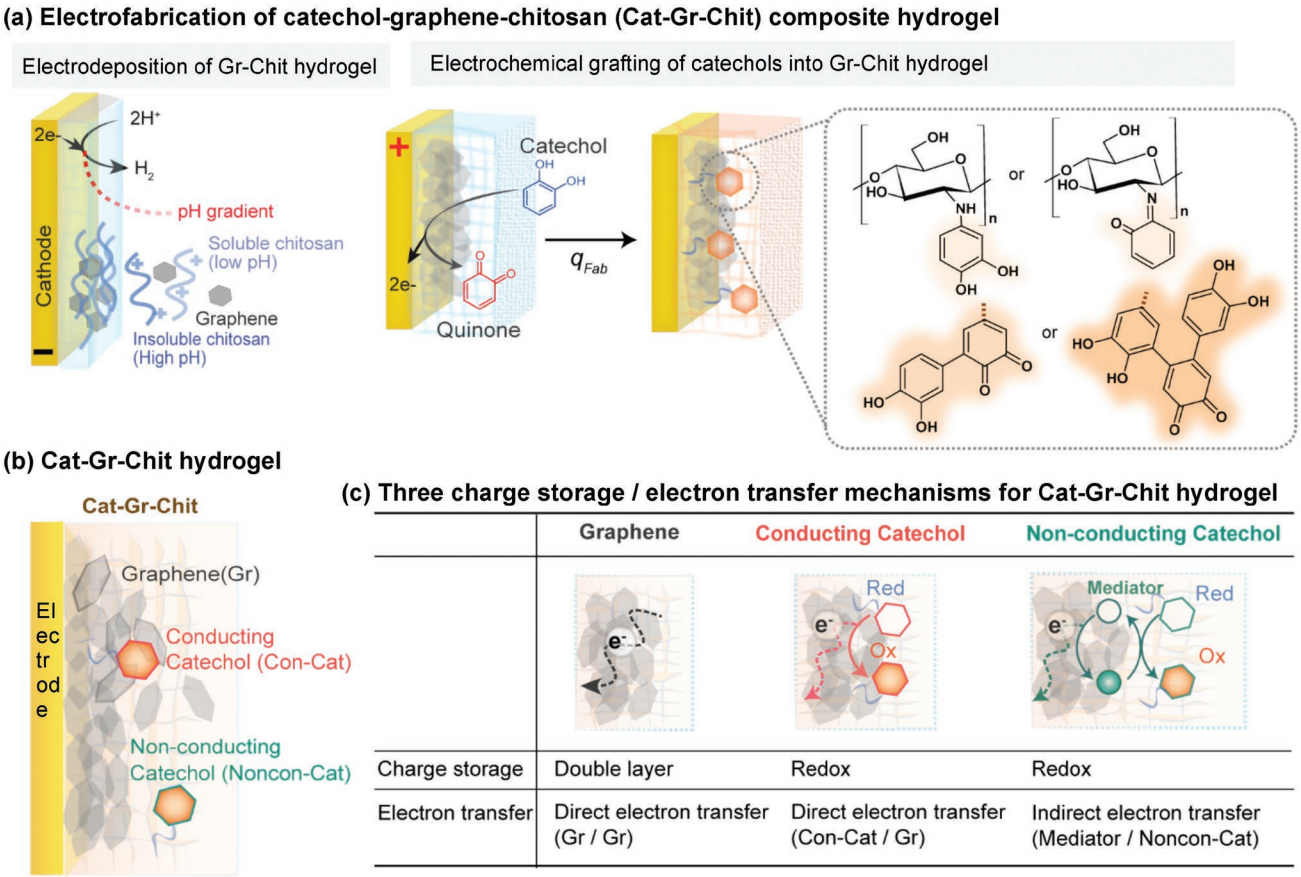

Scheme 1. a) Two-step electrofabrication of Cat-Gr-Chit composite hydrogel film. b) Proposed structure to explain functional properties: the composite contains conducting graphene and two catechol populations. c) Proposed mechanisms for charge-storage and electron-transfer for Cat-Gr-Chit composite hydrogel.

storage,[25–33] optoelectronics,[34–36] organic electronics,[7,37,38] and bioelectronics.[12,39–41] Interestingly, the characterization of redox polymers often focuses on their conducting properties although some recent studies found that the addition of diffusible redox mediators can enhance their functional capacities (e.g., for charge storage and molecular memory).[42–44] While various composite materials systems have been prepared from carbon-based nanomaterials, redox polymers, and in some cases, redox mediators,[45–48] the electron-transfer mechanisms within these composites are not fully resolved.

Here we prepared an electrode coated with a hydrogel film containing both catechol (Cat) and graphene (Gr), and report that it possesses synergistic properties. **Scheme 1**a illustrates that the catechol-graphene-chitosan (Cat-Gr-Chit) composite hydrogel is assembled on the electrode surface by two electrofabrication steps. First, the graphene-chitosan (Gr-Chit) hydrogel is electrodeposited from a slightly acidic suspension of graphene and the pH-responsive film-forming aminopolysaccharide chitosan.[49] Chitosan is commonly used to co-deposit nanoparticles since a negative electrode potential can lead to a locally high pH that induces chitosan to self-assemble into a hydrogel film that entraps the particles.[50–53] Second, catechol is oxidatively-grafted to the chitosan by immersing the Gr-Chit-coated electrode into a catechol solution and imposing a positive potential (relative to catechol's E^0) to the underlying electrode to generate the reactive quinones that chemically graft to chitosan (note: q_{Fab} is the number of electrons transferred during this anodic oxidation and serves as a measure of the extent of catechol modification).[6,54] Scheme 1a suggests putative chemical structures for the oxidatively grafted catechol monomers and oligomers[55] although the complexity of this chemistry eludes a full characterization just as for the related melanin[56,57] and polydopamine materials.[58,59] These two electrofabrication steps are simple and rapid, and allow films to be prepared with controlled compositions (the graphene content is controlled by deposition time, t, in the first step, while the catechol content is controlled by the oxidation charge, q_{Fab}, in the second step).

We report that the catechol and graphene components in the composite film (Scheme 1b) enable different mechanisms for charge-storage and electron-transfer within the composite. The leftmost panel in Scheme 1c illustrates that the incorporation of graphene within the hydrogel enables charge-storage through a double layer mechanism and electron-transfer through a metal-like conductivity mechanism. Scheme 1b hypothesizes two functionally different populations of catechol. One population, the "conducting catechols", is believed to be in intimate contact with graphene and can directly exchange electrons with graphene. The central panel in Scheme 1c illustrates that these conducting catechols allow charge-storage through a redox

mechanism and can undergo direct electron-transfer with the graphene. The second population, the "non-conducting catechols", is believed to be grafted to the chitosan but physically separated from graphene and thus precluding direct electron exchange as previously demonstrated with the catechol-grafted chitosan.[60–62] The rightmost panel in Scheme 1c illustrates that these non-conducting catechols also allow charge-storage through a redox mechanism but require mediators (diffusible electron shuttles) to allow electron-exchange (either with the graphene or underlying electrode).[60,61] We characterize the redox-based electron-transfer using a spectroelectrochemical technique that can simultaneously measure electron transfer into/from the film and the switching of the film's redox-state.[6,63,64]

We report that these different charge-storage and electron-transfer mechanisms endow the Cat-Gr-Chit composite hydrogel film with synergistic functional properties. Specifically, the composite has a graphene-based double layer capacitance and a catechol-based redox-capacitance. Further, the Cat-Gr-Chit hydrogel retains both the conducting properties of graphene and the molecular switching properties of catechol. Finally, we demonstrate the important role that mediators can play in controlling electron flow through redox-active films. We envision this molecular-mechanism-level understanding of redox-activities will enhance our ability to design electronic materials for diverse technological applications.

2. Results and Discussions

2.1. Materials Characterization

To characterize the microstructure of various composite hydrogels, we employed scanning electron microscopy (SEM). For this, we electrofabricated a Chit- or Gr-Chit-hydrogel on an electrode surface by electrodepositing from either a chitosan solution (1 w/v%) or a blend of chitosan and graphene (1 w/v%) using a constant current density of 0.6 mA cm^{-2} for 3 min.

The catechol-modified hydrogels (Cat-Chit or Cat-Gr-Chit) were then prepared by performing the oxidative-grafting of catechol onto the Chit or Gr-Chit-coated gold electrode (10 mM catechol, q_{Fab} = 0.32 C cm^{-2}). After that, the catechol-grafted hydrogel electrodes were washed with excess water to remove the physically bound catechols on the surface. **Figure 1**a compares the SEM images of these various films. The SEM images for the Chit- and Cat-Chit hydrogels are generally featureless while those for the Gr-Chit and Cat-Gr-Chit hydrogels show the uniformly distributed and crumpled graphene flakes.[65] Also, Figure 1a shows no significant change in the SEM image of Cat-Gr-Chit hydrogel compared with Gr-Chit hydrogel. Therefore, the SEM images of Figure 1a indicate that the microstructure of graphene is maintained after two processes of the electrodeposition of chitosan and the oxidative grafting of catechol to chitosan.

Initial chemical characterization of electrofabricated hydrogels was performed using UV–VIS spectroscopy. To facilitate the optical analysis, we prepared hydrogels with a lower graphene content by electrodepositing from a chitosan solution (1 w/v%) containing only 0.2 w/v% graphene using a transparent gold electrode and applying the constant current density (0.6 mA cm^{-2}) for a short time (90 s). Figure 1b shows the UV–VIS spectra and photographs of the various hydrogel-coated transparent gold electrodes. While the clear Chit-hydrogel coated electrode shows very low absorbance, the Gr-Chit hydrogel coated electrode is light gray and shows broadband absorbance (≈0.6) over the entire wavelength region. This absorbance of the Gr-Chit hydrogel is presumably due to π–π^* transition of sp^2 C=C bonds through the π-conjugation network of graphene.[66,67] The brown-colored Cat-Chit hydrogel coated electrode shows higher absorbance at the lower wavelengths consistent with previous reports for catechol-modified chitosan hydrogel.[6,63] Interestingly, the Cat-Gr-chit hydrogel shows the combined UV–VIS spectra of Gr-Chit and Cat-Chit-hydrogel coated electrode: i) the high absorbance over the entire wavelength range like Gr-Chit hydrogel; and ii) the higher absorbance in the lower wavelength region like Cat-Chit-hydrogel. This result indicates that the Cat-Gr-Chit hydrogel contains optical absorbance features of both the graphene and the grafted catechols

Figure 1c shows the Raman spectra for Gr(1%)-Chit and Cat-Gr(1%)-Chit hydrogel coated electrodes that were prepared using the same high Gr-content deposition solution as used for the SEM experiment. Both hydrogels show the characteristic *D*-band (≈1334 cm^{-1}) and *G*-band (1576 cm^{-1}) for graphene which are related to structural defects in the hexagonal sp^2 carbon lattice (*D*-band) and to edge defects (*G*-band).[68] Figure 1c shows the small increase of the I_D/I_G ratio in Cat-Gr-Chit (I_D/I_G = 1.11) with respect to the Gr-Chit (I_D/I_G = 1.07), which suggests the possibility that the electrofabrication steps may induce local defects in graphene structure.[69]

As another chemical characterization method, we used FT-IR spectroscopy as shown in Figure 1d. Each hydrogel was electrofabricated and then peeled from the electrode surface and suspended in water.[70] The spectrum for the Chit-hydrogel shows the characteristic broad peak at ≈3000 cm^{-1} that includes −OH, and −NH stretching vibrations (labeled "Band 1"). The Cat-Chit hydrogel shows the appearance of multiple peaks between 1700 and 1200 cm^{-1} (Band 2: C=C stretching vibration of benzene) and a comparative decrease in the peak at 1050 cm^{-1} (Band 3: C−O stretching vibration).[71,72] The spectrum for the Gr-Chit-hydrogel shows few distinguishing features, while the spectrum of Cat-Gr-Chit hydrogel shows the increases of peaks between 1680 and 1200 cm^{-1} (Band 2) that is consistent with the spectrum of Cat-Chit-hydrogel. Also, the Band 2/Band 3 ratio is increased in the Cat-Gr-Chit hydrogel (compared to the Cat-Chit hydrogel), which could be attributed to π–π interactions between the catechol-derived species and graphene.[73]

In addition to structural and chemical characterizations of composite hydrogel, we employed electrochemical impedance spectroscopy (EIS) to characterize the electrical properties of hydrogel interfaces.[48,74–77] While EIS measurements tend to be very sensitive, relating the observed electrical properties (i.e., capacitance and resistance) to the underlying molecular-level phenomena (i.e., reaction and diffusion) can be challenging and thus various methods have been used for data interpretation.[78] Experimentally, we performed EIS measurements using a frequency range from 0.05 Hz to 10 kHz with a perturbation amplitude of 5 mV from the open circuit potential.

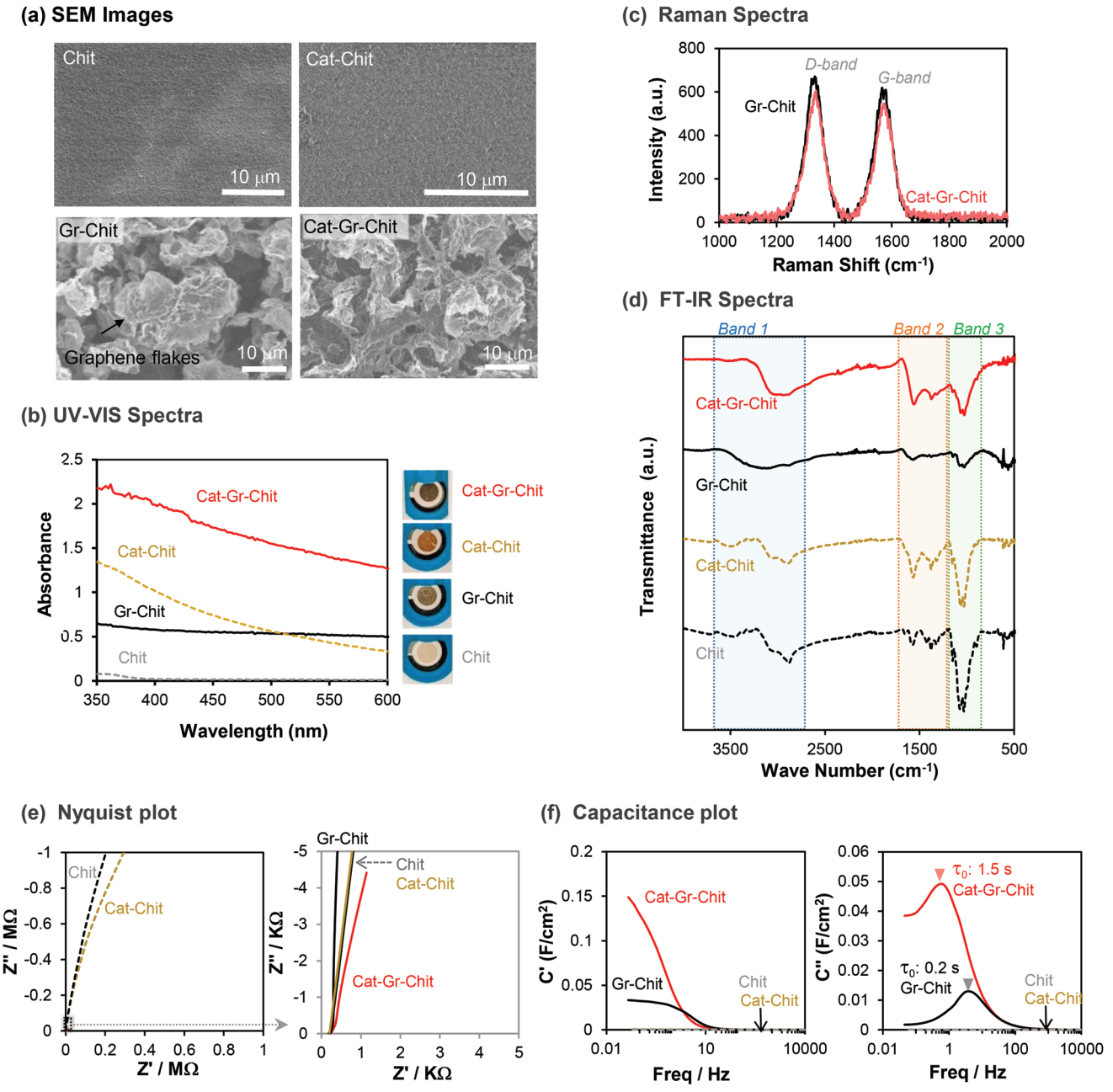

Figure 1. Materials characterization of Cat-Gr-Chit composite hydrogel. a) SEM images of electrofabricated hydrogels on a gold electrode. b) UV–VIS spectra and images of electrofabricated hydrogels on the transparent gold electrode. c) Raman spectra of Gr-Chit and Cat-Gr-Chit hydrogel electrofabricated on a gold electrode. d) FT-IR spectra of electrofabricated hydrogels. e) Nyquist plots from electrochemical impedance spectroscopy (EIS). f) Real (C′) and imaginary (C″) capacitance plots from EIS analysis.

The Nyquist plots in Figure 1e provide one approach to compare the behavior of the various hydrogels. The left plot of Figure 1e shows that the real part (Z′) and imaginary part (Z″) of impedance for hydrogels lacking Gr (i.e., Chit and Cat-Chit) are ≈500-fold larger than hydrogels containing Gr (i.e., Gr-Chit and Cat-Gr-Chit). The right plot of Figure 1e focuses on the low Z′ and Z″ region and shows that the two hydrogels lacking Gr show nearly identical response that is different from the hydrogels containing Gr. A small difference between the Gr-Chit and Cat-Gr-Chit hydrogel might be due to the charge transfer resistance that occurs in the Cat-Gr-Chit hydrogel. This Nyquist analysis suggests Gr confers conductivity to the films while the effect of catechol is less certain.

Figure 1f shows the frequency-dependent capacitance plot (note: Figure S1, Supporting Information, provides the Bode plots and the calculation of capacitance of Figure 1f). In the left plot of Figure 1f, at the lowest frequency (50 mHz), the real capacitance (C′) reaches the highest capacitance for each film. The hydrogels containing Gr show 300 times higher C′ capacitance compared with the Gr-lacking hydrogels. Also,

Cat-Gr-Chit is 4.3 times higher capacitance than Gr-Chit. This increase might result from the additional contribution of catechols into the Gr-Chit. The right plot of Figure 1f shows the sharp peak of imaginary capacitance (C″) at frequency (f_0). From f_0, the relaxation time (τ_0) for discharging is calculated as $\tau_0 = 1/f_0$.[79] A slower response is observed in Cat-Gr-Chit ($\tau_0 = 1.5$ s) compared with Gr-Chit ($\tau_0 = 0.2$ s), which might be due to the electron transfer to catechols.

In summary, the characterization results of Figure 1 support the conclusion that the electrofabricated Cat-Gr-Chit composite hydrogel possess both catechol and graphene components. Also, the EIS results for Gr-lacking hydrogels and Gr-containing hydrogels indicate that graphene can confer conductivity to the hydrogel. In addition, the difference in EIS results for Gr-Chit and Cat-Gr-Chit hydrogel suggests that the grafting of catechol to Gr-Chit hydrogel alters the electrical property of Gr-Chit hydrogel.

2.2. Mechanisms for Charge-Storage and Electron-Transfer without Mediators

2.2.1. Electrochemical Characterization of Conducting Catechol

To further characterize how the conductivity (conferred by graphene) and redox activity (conferred by catechol) affect the properties of the composite hydrogel, we measured the electrochemical behavior of hydrogels films prepared with different compositions. In the first study, we electrofabricated a thick hydrogel (≈25 µm as measured by SEM after freeze-drying) by: i) electrodepositing from a graphene (0.5%)–chitosan (1%) solution using a constant current (0.6 mA cm^{-2}; 3 min); and ii) anodic grafting by transferring this hydrogel-coated electrode to a catechol (10 mM) solution and applying a constant potential (+0.6 V versus Ag/AgCl) to achieve the oxidative charge (q_{Fab}) of 0.6 C cm^{-2}. **Figure 2**a compares the CVs of this Cat-Gr-Chit hydrogel-coated electrode, with CVs for control hydrogels all measured in phosphate buffer (PB; 0.1 M, pH 7.0). The CVs for the Chit- and Cat-Chit controls appear as horizontal lines, which indicate a non-conductive hydrogel. The CV for the Gr-Chit control hydrogel has a rectangular shape which indicates a capacitive hydrogel with a significant electrical double layer (EDL).[2,3,42,80] Presumably, this high EDL charge of Gr-Chit hydrogel compared with Chit hydrogel is due to the increase in conducting surface area conferred by the graphene entrapped in the hydrogel.

The CV for the Cat-Gr-Chit hydrogel shows a markedly different shape with 3 reduction peaks and the corresponding 3 oxidation peaks. These redox peaks suggest redox-active molecules (i.e., catechols) are bound to the conducting surface (i.e., to graphene) and electrons can be directly transferred from/to the conducting catechols.[81–83] Note: in Figure S2, Supporting Information, the CV for the Cat-Chit hydrogel shows no such peaks in the absence of Gr indicating that the direct electron transfer between catechol and the gold electrode is negligible. The appearance of multiple redox peaks could be due either to catechol's different redox states (catechol, semiquinone, and quinone) or various redox-active forms of grafted catechol (e.g., catecholic oligomers) that could be formed during oxidative electrofabrication.[55]

To quantitatively compare the capacitive and redox charges, Figure 2b shows that we analyzed the CV data as time series and calculated the charge by integrating the current over time. The schematic of Figure 2b illustrates that the total oxidative

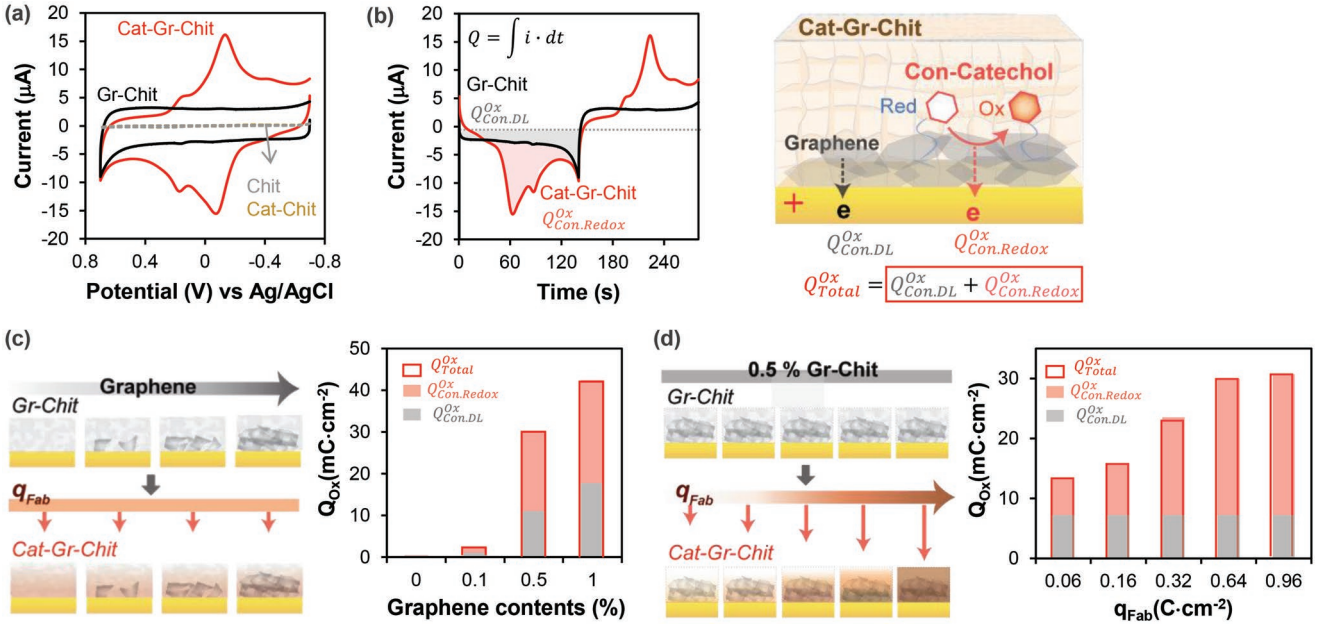

Figure 2. Electrochemical characterization without mediators. a) Cyclic voltammograms (CV) of 4 composite hydrogel-coated electrodes in phosphate buffer (scan rate of 10 mV s^{-1}). b) Current–time plots for Gr-Chit and Cat-Gr-Chit composite hydrogel were used to quantify the oxidative charge to form the electrical double layer ($Q^{Ox}_{Con.DL}$) and to switch the redox-state of the conductive catechols ($Q^{Ox}_{Con.Redox}$). c) The effect of graphene on the oxidative charge-transfer mechanisms. d) The effect of catechol (q_{Fab}) on the oxidative charge-transfer mechanisms.

charge (Q^{Ox}_{Total}) of Cat-Gr-Chit hydrogel is considered to be the sum of the double layer and redox oxidative charge. The oxidative charge associated with the conductive EDL (grey area, $Q^{Ox}_{Con.DL}$) was estimated from the results with the Gr-Chit film, while the conductive redox oxidative charge (red area, $Q^{Ox}_{Con.Redox}$) was estimated from the difference in oxidative charge between the Cat-Gr-Chit and the Gr-Chit hydrogels as described in Figure 2b.

First, we examined the effect of graphene content. For this, we electrofabricated Gr-Chit hydrogels with different graphene levels by immersing the electrodes into chitosan (1%) solutions mixed with different graphene contents (0, 0.1%, 0.5%, 1%) and then applied a constant current of 0.6 mA cm^{-2} for 3 min. As expected, the subsequent CV measurements with these Gr-Chit hydrogels (Figure 2c) show that $Q^{Ox}_{Con.DL}$ increased with graphene content presumably due to an increase in conductive surface area and corresponding double layer capacitance. After these CV measurements, the hydrogel-coated electrodes were immersed into a catechol (10 mM) solution and a constant potential of +0.6 V was imposed to achieve the oxidative charge (q_{Fab}, 0.32 C cm^{-2}). CV measurements with these Cat-Gr-Chit hydrogels allowed calculation of the total oxidative charge $\left(Q^{Ox}_{Total}\right)$ and the conductive oxidative charge attributed to the conducting catechol $\left(Q^{Ox}_{Con.Redox} = Q^{Ox}_{Total} - Q^{Ox}_{Con.DL}\right)$ which are shown as the colored bars in Figure 2c (note: Figure S2, Supporting Information, provides CV results for all hydrogels). As can be seen from Figure 2c, catechol alone (Gr = 0%) conferred neither a double layer nor a redox charge to the film. In the presence of Gr, hydrogels of the same catechol content showed increases in conductive redox charge ($Q^{Ox}_{Con.Redox}$) with increases in the graphene content. These results are consistent with a mechanism in which catechols can associate with graphene within the film to confer a redox conductivity, but in the absence of graphene, the catechols cannot directly exchange electrons with the electrode.

Next, we examined the effect of the grafted catechol level. For this, we prepared 5 identical Gr-Chit hydrogel coated electrodes by electrodepositing from a chitosan (1%) solution containing 0.5% graphene using a cathodic current density of 0.6 mA cm^{-2} for 3 min. After that, we measured CVs of five Gr-Chit-hydrogel coated electrodes in buffer solution and calculated the conductive DL charge ($Q^{Ox}_{Con.DL}$) which are shown in grey in Figure 2d. Using the same 5 Gr-Chit hydrogel coated electrodes, we electrochemically grafted different levels of catechol by immersing the Gr-Chit coated electrodes in a catechol (10 mM) solution and imposing a positive voltage of +0.6 V (versus Ag/AgCl) for differing times to achieve oxidative charge (q_{Fab}) that varied from 0.06 to ≈0.96 C cm^{-2}. After that, CV experiments for 5 Cat-Gr-Chit coated electrodes were performed in buffer and the conductive redox charge ($Q^{Ox}_{Con.Redox}$) is calculated by subtracting the DL charge ($Q^{Ox}_{Con.DL}$) of Gr-Chit coated electrode from the total charge (Q^{Ox}_{Total}) of Cat-Gr-Chit coated electrode. Figure 2d shows that the conductive redox charge ($Q^{Ox}_{Con.Redox}$) monotonically increased with q_{Fab} up to a q_{Fab} of 0.96 C cm^{-2}. An apparent saturation effect was observed from 0.6 to 0.96, and potentially, this could be due to a limitation in the available graphene surface area for catechol association.

In conclusion, the results of Figure 2 demonstrate that graphene is essential for the double layer charging and is also essential for the conductive redox charging that is conferred by catechol. These results support the mechanism proposed in Scheme 1 in which conducting catechols can directly transfer electrons through an interconnected graphene network.

2.2.2. Molecular Switching of Conducting Catechol

To characterize the conductive redox electron transfer through the Cat-Gr-Chit composite hydrogel (central panel of Scheme 1c) we performed dynamic time series spectroelectrochemical measurements to detect redox-state switching of the conducting catechols while electrons are being transferred into/from the film.[64,84] To allow the measurement of optical absorbance, we used a transparent gold electrode and modified our electrodeposition conditions to deposit a thin (≈5 µm), partially-transparent Gr-Chit hydrogel film. Specifically, we electrodeposited using a chitosan solution (1%) with a lower level of graphene (0.2%) and imposed the cathodic current (0.6 mA cm^{-2}) for a relatively short time (90 s). This thin Gr-Chit hydrogel coated electrode was then immersed into a catechol (10 mM) solution and a positive potential (+0.6 V versus Ag/AgCl) was applied to achieve an anodic charge (q_{Fab}) of 0.3 C cm^{-2} to generate the Cat-Gr-Chit hydrogel. For spectroelectrochemical measurements, **Figure 3**a shows that this thin hydrogel coated electrode was immersed in a cuvette containing phosphate buffer (PB; 0.1 M, pH 7.0), the cuvette was then placed into the instrument, and an oscillating potential input was applied to the electrode. The two outputs (electrical current and optical absorbance) were simultaneously measured.

Figure 3b compares the time series electrical and optical outputs for the Cat-Gr-Chit film to those for a control Gr-Chit film lacking catechol (shown in grey). Note: Figure S3, Supporting Information, shows time series outputs of additional control films of Chit and Cat-Chit. The first output curve in Figure 3b is the electrical current. The Cat-Gr-Chit composite hydrogel shows higher oscillating current peaks compared to the Gr-Chit hydrogel. A second, electrical, output in Figure 3b is the charge which is calculated by integrating the current output over time ($Q = \int i \times dt$). The Cat-Gr-Chit film shows the output charge oscillates with a larger amplitude ($\Delta Q_{Cat.Gr.Chit}$ = 2.8 ± 0.06 mC) compared to that for the control Gr-Chit film ($\Delta Q_{Gr.Chit}$ = 1.0 ± 0.01 mC). Presumably, the larger amount of charge being transferred for the Cat-Gr-Chit (versus the Gr-Chit hydrogel) reflects an additional redox-based electron transfer mechanism.

The third output in Figure 3b is the optical absorbance (480 nm) associated with the redox state of the grafted catechol moieties.[6,11] The Cat-Gr-Chit hydrogel shows an oscillating absorbance output ($\Delta A_{Cat.Gr.Chit}$; 0.019 ± 0.002), while the control Gr-Chit hydrogel shows no oscillations in the absorbance output ($\Delta A_{Gr.Chit}$; ≈0). This oscillating output absorbance provides direct evidence that the redox state of some catechol moieties (i.e., the "conducting catechols") are being repeatedly switched between their reduced (catechol) and oxidized (quinone) states by electron transfer through the graphene network (note: Figure S3a, Supporting Information, shows the output absorbance does not oscillate for a Cat-Chit film that lacks Gr).

It is interesting to note two additional features of the time series input–output curves in Figure 3b. First, the electrical and

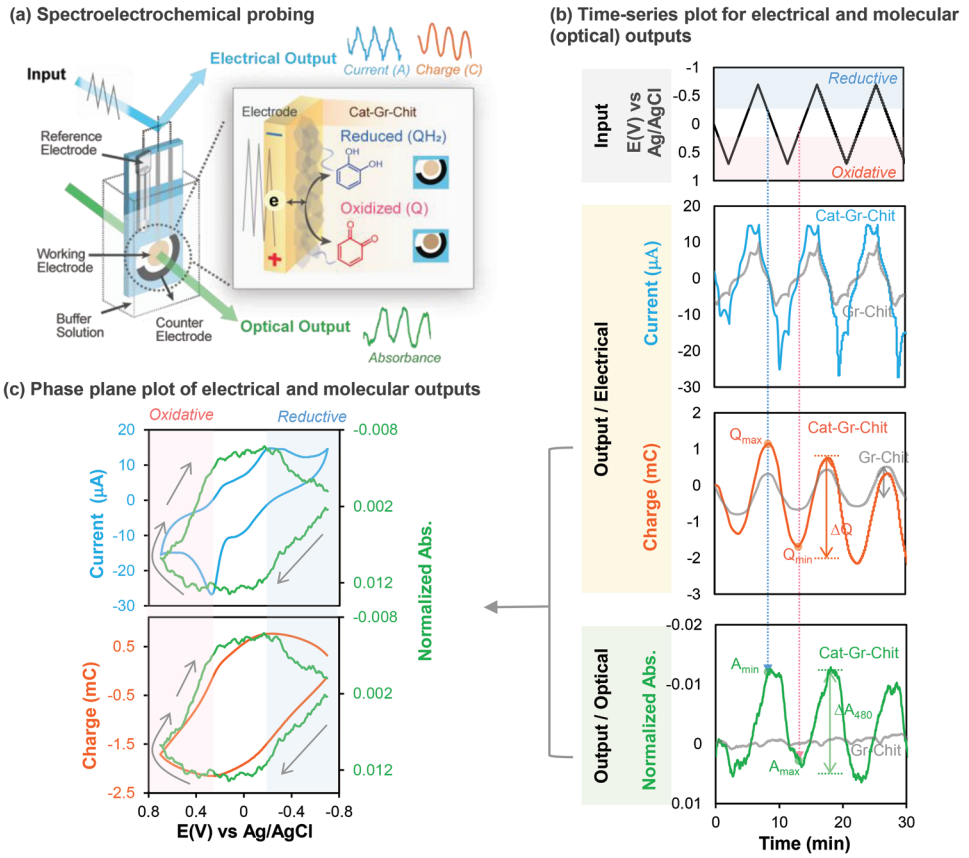

Figure 3. Molecular switching without mediators (detect the conducting catechols). a) Schematic for a spectroelectrochemical probing of the composite films: oscillating potential inputs induce cyclically varying electron-flow (electrical output) and redox-state switching of the grafted catechols (optical output). b) Time series output curves of the response to cyclically-oscillating input potential in buffered solutions without mediators (note: the absorbance is normalized by subtracting the initial absorbance to emphasize its change). c) Phase-plane plots showing how the input potential affects the flow of electrons (measured as current or charge) and molecular redox-state switching of the grafted catechols (as measured by optical absorbance).

optical outputs appear to be steady over time (i.e., the current, charge, and absorbance amplitudes appear nearly constant for these 3 cycles). This behavior will be further discussed later. Second, the oscillating output charge (Q) and absorbance (A) appear to be in-phase with each other, but out-of-phase with the input potential. Specifically, the dotted vertical lines in Figure 3b illustrate that the maximum (i.e., reductive) charge (Q_{max}) occurs at the same time as the minimum absorbance (A_{min}, associated with the reduced catechol state), and the minimum (i.e., oxidative) charge (Q_{min}) occurs at the same time as the maximum absorbance (A_{max}, associated with the oxidized quinone state).

To facilitate interpretation, it is common to display time series data as phase plane plots of output versus input potential.[11,12] The first phase plane plot of Figure 3c shows the electrical current and optical absorbance output responses as a function of imposed potential. When the potential was swept into the oxidative region (approximately +0.3 V versus Ag/AgCl), the optical absorbance was observed to increase which is consistent with the switching of the catechol to the oxidized quinone. When the potential was swept into the reductive region (approximately –0.2 V versus Ag/AgCl) the absorbance was observed to decrease consistent with the switching of quinone to the catechol.

The second phase plane plot of Figure 3c shows the charge and absorbance output responses. The shapes of these two phase plane plots are nearly superimposable further illustrating the strong correlation between the charge transfer from the electrode and the molecular switching of the redox state of the conducting catechols in the Cat-Gr-Chit hydrogel. Importantly, the phase plane plot for the Cat-Chit film lacking Gr shows no molecular switching (see in Figure S3b, Supporting Information). In summary, these spectroelectrochemical measurements demonstrate direct electron transfer to switch the redox state of the conducting catechols.

2.3. Mechanisms for Charge-Storage and Electron-Transfer with Mediators

2.3.1. Molecular Switching of Non-Conducting Catechol

While the above results provide evidence for a population of conducting catechols that can directly exchange electrons with Gr (illustrated by the center panel of Scheme 1c), we report that there is a second functional population of catechols that remains redox-active but cannot directly exchange electrons with Gr (illustrated by the right panel of Scheme 1c).

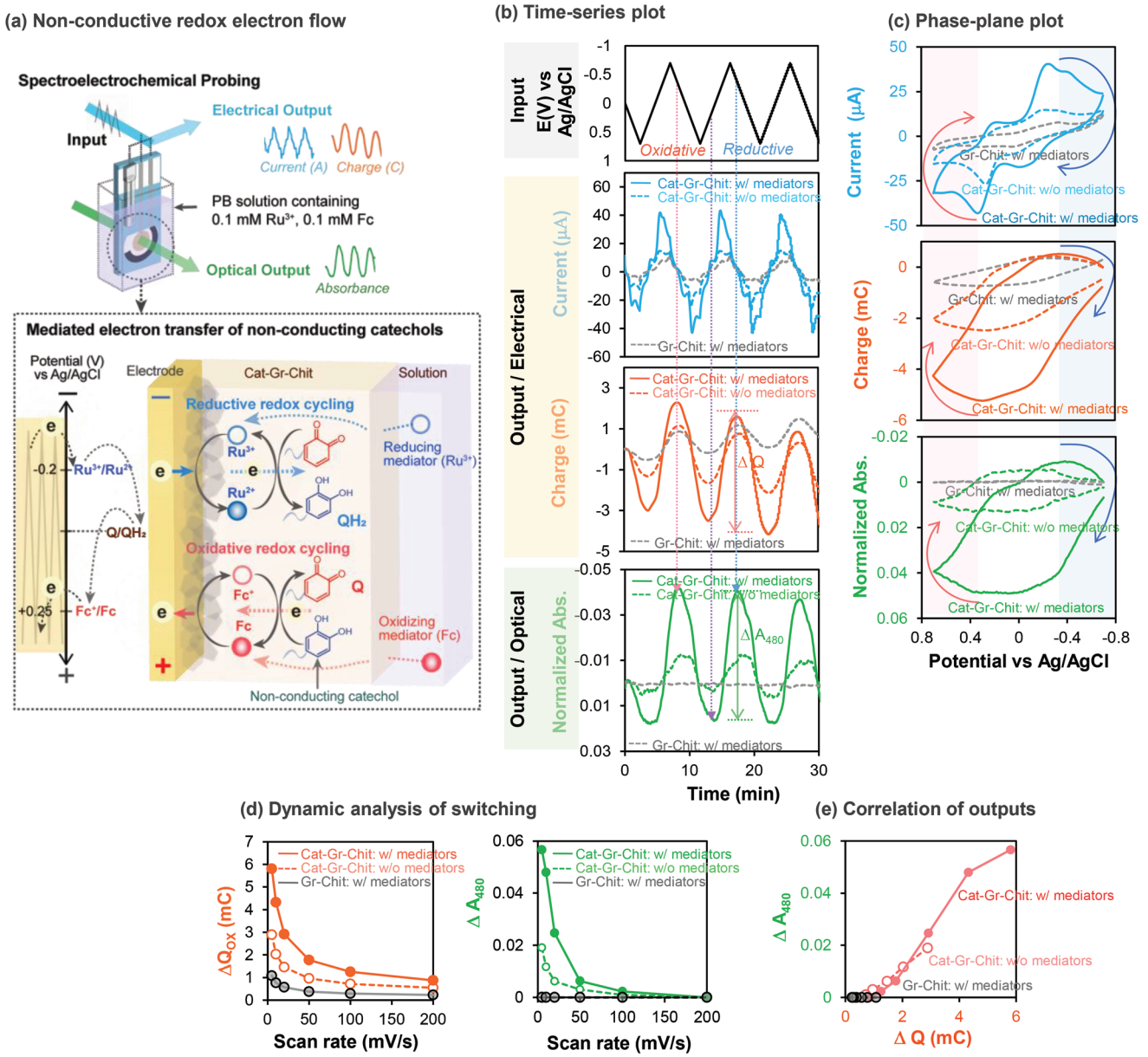

Figure 4. Molecular switching with mediators (detect the non-conducting catechols). a) Schematic of spectroelectrochemical probing when diffusible mediators are used to shuttle electrons to/from the non-conducting catechols through redox-cycling mechanisms. b) Time series output curves of the response to cyclically oscillating input potential in buffered solutions (PB) without or with mediators (0.1 mM ferrocene dimethanol [Fc] and 0.1 mM ruthenium hexamine chloride [Ru^{3+}]). c) Phase-plane plots showing how the catechol and mediators alter the output electrical (current and charge) and optical (absorbance) responses due to the redox-state switching of the grafted catechols. d) Dynamic analysis of the electrical and optical outputs as a function of scan rate (e.g., frequency). e) Cross-correlation illustrates the importance redox-state switching of the catechol (measured as ΔA) to the ability to transfer electrons into/from the composite (measured as ΔQ).

Specifically, we envision these "non-conducting" catechols are covalently grafted to the chitosan matrix but do not form the associations with Gr that enable direct electron transfer.

To reveal this second functional population of catechols, we performed a second set of spectroelectrochemical measurements using the same thin hydrogel coated electrodes in Figure 3, but this time using a buffered solution containing two mediators (i.e., diffusible electron shuttles). These two mediators sequentially engage the non-conducting catechols in redox-cycling reactions as illustrated by the scheme of **Figure 4**a. When the electrode-imposed potential is cycled to the oxidative region, the ferrocene dimethanol (Fc) mediator undergoes oxidative redox-cycling to switch the non-conducting catechols to their oxidized (e.g., quinone) state. When the electrode-imposed voltage is cycled to the reductive region, the $Ru(NH_3)_6Cl_3$ (Ru^{3+}) mediator undergoes reductive redox-cycling to switch the non-conducting catechols to their reduced (e.g., catechol) state.

Figure 4b shows time series curves for multi-cycle CV measurements for the Cat-Gr-Chit hydrogel probed in the presence of the Fc and Ru^{3+} mediators (0.1 mM each) and compares this output response to that observed for the same film probed

without mediators (i.e., output curves from Figure 3b are reproduced in Figure 4b while Figure S4, Supporting Information, shows results from various additional control films). The first set of output curves in Figure 4b show the electrical current. The largest currents were observed when the Cat-Gr-Chit composite hydrogel was probed in the presence of both mediators. The amplified currents for the Cat-Gr-Chit hydrogel in the presence (versus absence) of mediators are consistent with the existence of a second population of catechol that is non-conducting and requires diffusible mediators to induce their redox-switching.

The second set of outputs in Figure 4b is the electrical charge (Q). Again, the largest amplitude for the oscillating Q was observed when the Cat-Gr-Chit composite film was probed with both mediators ($\Delta Q^{Mediator}_{Cat.Gr.Chit}$; 5.8 ± 0.02 mC) and this value is considerably larger than the values observed when probing the same Cat-Gr-Chit hydrogel without mediators ($\Delta Q^{PB}_{Cat.Gr.Chit}$; 2.8 ± 0.06 mC) or for probing the Gr-Chit hydrogel with mediators ($\Delta Q^{Mediator}_{Gr.Chit}$;1.0 ± 0.02 mC). This increase in ΔQ indicates that the mediators allow more electrons to be transferred into and from the Cat-Gr-Chit film during each CV cycle, and this result is consistent with a population of redox-active but non-conducting catechol moieties in the film.

The third set of output curves in Figure 4b is the optical absorbance associated with the catechol moieties' redox state. The amplitude of the oscillating optical absorbance output (ΔA) provides a semi-quantitative measure of the redox-state switching of the catechol moieties. As expected, the Gr-Chit film that lacks catechol moieties shows no oscillations in absorbance ($\Delta A^{Mediator}_{Gr.Chit}$; 0). Figure 4b shows the oscillating optical absorbance for the Cat-Gr-Chit film is significantly larger when probed with mediators ($\Delta A^{Mediator}_{Cat.Gr.Chit}$; 0.05 ± 0.003) than without mediators ($\Delta A^{PB}_{Cat.Gr.Chit}$; 0.015 ± 0.002). Comparison of these absorbance amplitudes suggests that for this Cat-Gr-Chit hydrogel, 1/3 of the redox-active catechols are conducting and 2/3 are non-conducting, approximately.

Figure 4c displays the electrical and optical phase plane plots for this CV data. When the Cat-Gr-Chit hydrogel was probed with mediators, the upper output plot shows a significant current amplification compared to probing this hydrogel without mediators or probing a Gr-Chit hydrogel with mediators. The positions for the various oxidation and reduction peaks are also shown in the upper plot of Figure 4c. Intuitively, it is expected that this plot should show peak positions associated with both the conducting catechols and also the Fc ($E^{0,Fc}$ = +0.25 V) and Ru^{3+} ($E^{0,Ru3+}$ = –0.2 V) mediators. However, because of the overlap of these potential values, these peaks cannot be unambiguously discerned.

The middle and lower plots in Figure 4c show the Q and A phase plane plots. As seen in Figure 3c, the shapes of the Q and A phase planes are nearly superimposable for the Cat-Gr-Chit hydrogel which shows a strong correlation between electron transfer and the molecular switching of the catechol moieties independent of whether mediators are used for switching. However, the larger amplitude observed when the Cat-Gr-Chit hydrogel was probed with mediators is consistent with the mediators switching a larger population of catechols.

To further compare the response of the conducting and non-conducting catechols, we performed dynamic analysis by probing the Cat-Gr-Chit hydrogel in the presence and absence of mediators using varying scan rates (Figure S5, Supporting Information, provides the time series outputs of CV measured at different scan rates). Figure 4d shows that the amplitudes of the oscillating electrical output (ΔQ) and optical output (ΔA_{480}) both decrease with increasing scan rates. Figure 4e shows the cross-correlation between these output amplitudes. One observation is that this correlation appears linear suggesting that the electrons transferred to/from the hydrogel are associated with switching of the redox state of the catechols. Importantly, this line seems to have a similar slope irrespective of whether the hydrogel is probed with or without mediators, suggesting the same number of electrons is required to switch the conducting and non-conducting catechols. The x-intercept in Figure 4e suggests that ≈1 mC of charge may be associated with the double-layer capacitance associated with graphene.

Another important observation in Figure 4e involves the charge amplitude (ΔQ). The addition of Gr to a Chit hydrogel was observed to increase ΔQ from 0.22 (Chit; Figure S4, Supporting Information) to 1 mC (Gr-Chit). This increase is expected as Gr is expected to confer a double layer capacitance. The addition of catechol to the Gr-Chit film is observed to further increase ΔQ in a scan-rate dependent manner. The increase conferred by catechol is consistent with the addition of a redox capacitance. When the Cat-Gr-Chit film was probed without mediators, we hypothesize this redox capacitance is associated with the conducting catechols. When the Cat-Gr-Chit hydrogel was probed with mediators, we hypothesize the redox capacitance includes both the conducting and non-conducting catechols. Importantly, mediators are required to switch the non-conducting catechols to allow significantly more electrons to be transferred to/from the hydrogel and corresponding increases in ΔQ and ΔA_{480}.

2.3.2. Electrochemical Characterization of Non-Conducting Catechol

In the above experiments (Figures 3 and 4) we examined thin partially-transparent films with comparatively low levels of graphene and catechol to provide direct experimental evidence for the different charge-storage and electron-transfer mechanisms. We next examined the functional consequences of these three mechanisms for the thicker hydrogel films studied in Figure 2a.

In an initial characterization, we performed CV measurements in the presence or absence of the Fc ($E^{0,Fc}$ = +0.25 V versus Ag/AgCl) and Ru^{3+} ($E^{0,Ru3+}$ = –0.2 V versus Ag/AgCl) mediators. For the Gr-Chit hydrogel lacking catechol, **Figure 5**a shows small changes in the CV when mediators were added. Thus, for this Gr-Chit hydrogel, the mediators have little effect on the conducting mechanism conferred by graphene. In contrast, Figure 5a shows the CVs for the Cat-Gr-Chit hydrogel are dramatically different depending on whether mediators are added to access the redox-non-conducting catechols.

There are three observations from a comparison of the CVs for the Cat-Gr-Chit hydrogel probed with mediators (versus without mediators). First, large peak currents are observed at the mediator redox potentials (a small oxidation peak current around +0.5 V versus Ag/AgCl might be due to the Cl^- oxidation of $Ru(NH_3)_6Cl_3$[85]). This observation is consistent with

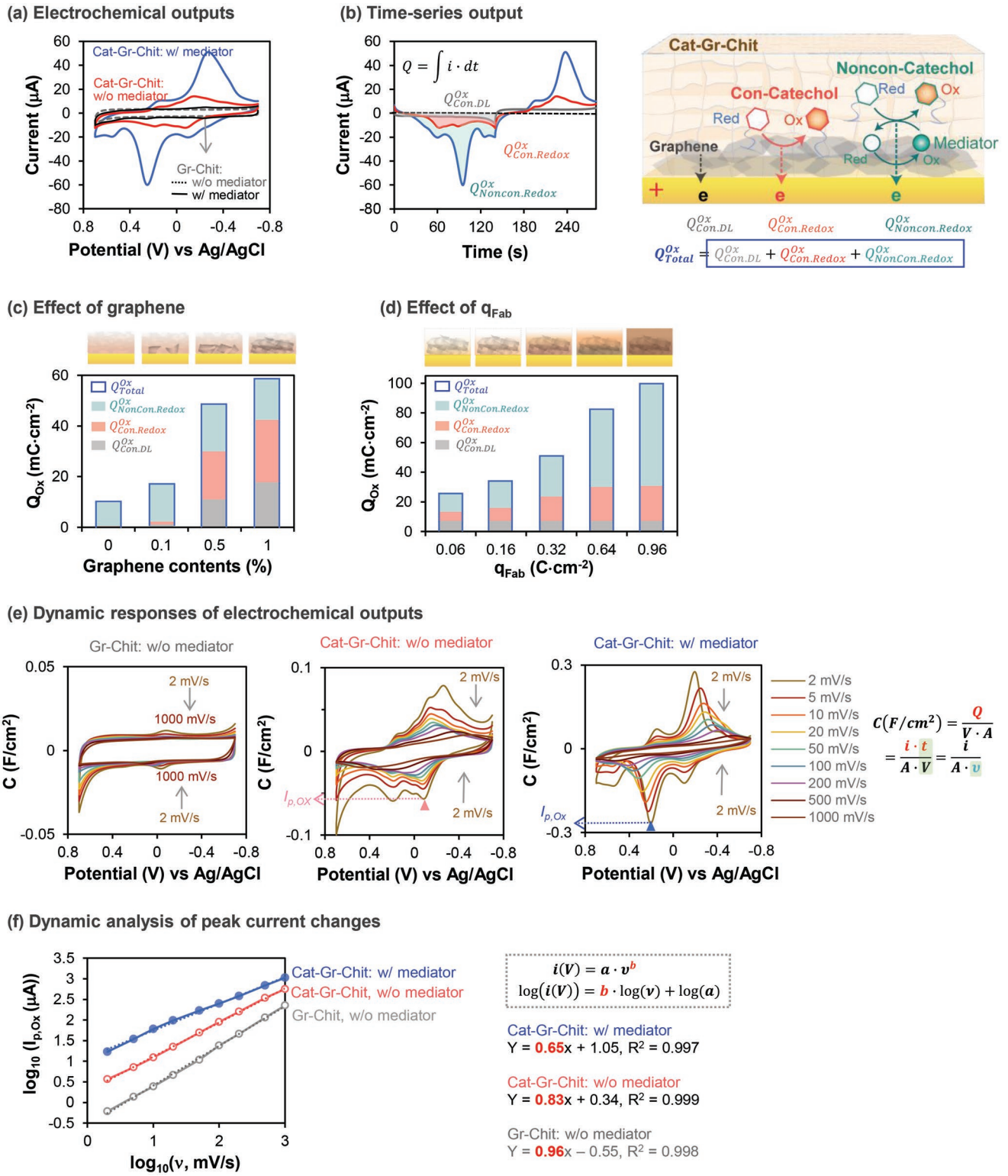

Figure 5. Electrochemical characterization with mediators. a) Cyclic voltammograms (CV) of graphene-containing composites when probed with or without mediators (0.1 mM Fc, 0.1 mM Ru^{3+}; scan rate of 10 mV s^{-1}). b) Current–time plots used to quantify the oxidative charges ($Q^{Ox}_{Con.DL}$, $Q^{Ox}_{Con.Redox}$, $Q^{Ox}_{NonCon.Redox}$). c) The effect of graphene on the oxidative charge-transfer mechanisms. d) The effect of catechol (q_{Fab}) on the oxidative charge-transfer mechanisms. e) Dynamic analysis in which output currents are converted to area capacitance values (C, F cm^{-2}: CVs performed from 2 to 1000 mV s^{-1}). f) Dynamic analysis of oxidation peak currents as a function of the scan rate.

the requirement for diffusible mediators to allow the non-conducting catechols to exchange electrons, and also illustrates the role of the mediators as voltage gates to allow electron flow to/from the non-conducting catechol population. Note: the role of the mediators to gate current flow from the non-conducting catechols is more apparent from CVs in Figure S6, Supporting Information, for studies with the Cat-Chit hydrogel that lacks Gr. Second, the mediator peak currents are amplified: the mediators can access the non-conducting catechol population that serves as an additional source/sink of electrons. Third, the mediator currents are rectified by the catechol: Fc-oxidation (but not Fc-reduction) is amplified and Ru^{3+}-reduction (but not Ru^{3+}-oxidation) is amplified. These molecular electronic properties (i.e., the amplification, rectification, and gating of currents) have been previously reported for redox-active but non-conducting films in bioelectronics applications.[11,60,62,86]

To estimate the relative contributions of three electron transfer mechanisms, Figure 5b shows that we integrated the time series current plots. Specifically, probing of the Gr-Chit hydrogel allows an estimate of double layer charge conferred by graphene ($Q^{Ox}_{Con.DL}$), probing of the Cat-Gr-Chit hydrogel without mediators allows an estimate of the conductive redox charge conferred by the conducting catechol's ($Q^{Ox}_{Con.Redox}$), and probing of the Cat-Gr-Chit film with mediators allows an estimate of the non-conductive redox charge conferred by the non-conducting catechol's ($Q^{Ox}_{NonCon.Redox}$).

Using the same thick hydrogels as those in Figure 2c,d, we performed probing studies with the Fc and Ru^{3+} mediator pair (note: Figure S7, Supporting Information, provides the CVs of various Cat-Gr-Chit hydrogels in the presence of mediators). The results summarized in Figure 5c show that when the hydrogel's graphene content was increased, both the double layer charge and the conductive redox charge increased, while the non-conductive redox charge was unchanged (Figure 5c, green component). When the catechol content of the hydrogels was increased, Figure 5d shows there was no effect on the conducting double layer charge (Figure 5d, gray component), while both the conductive redox charge and non-conductive redox charge increased. Interestingly, in the higher q_{Fab} region, the conductive redox charge appears to be limited by graphene, while the non-conductive redox charge is increased with catechol content. Importantly, these results indicate that the ability of the mediators to access the non-conducting catechol population leads to a large increase in electron exchange in the hydrogel.

Next, we performed dynamic analysis by probing these thick hydrogels at different scan rates from 2 to 1000 mV s^{-1}. To compare the response from multiple CVs using a similar *y*-axis scale, we converted the CV measurements into area capacitances by dividing the output charge (Q) by the electrode surface area and scan rate as described by the equation of Figure 5e (note: Figure S8, Supporting Information, provides the current output results of CVs measured at different scan rates). The first plot of Figure 5e shows CV results for the Gr-Chit hydrogel when probed in the absence of mediators and the shape of these curves is largely independent on the scan rate. These results are consistent with an EDL capacitance associated with graphene.[1,2] The second plot in Figure 5e shows the CV results for the Cat-Gr-Chit hydrogel when probed without mediators, and includes contributions from both graphene's double layer capacitance and the conducting-catechols redox capacitance. The final plot shows CV results for the Cat-Gr-Chit hydrogel when probed with mediators, which includes all three electron transfer mechanisms. These latter plots both show that the total capacitance decreases with increasing scan rate which is consistent with a redox capacitance mechanism.

To further characterize the dynamics of the electrochemical response, we examined how the peak current (i_p) varies with scan rate (ν).[2,87–89] The equations in Figure 5f show a power-law dependence with the exponent (b) providing mechanistic insights: b approaches 1 for surface-controlled electrochemical processes, and 0.5 for diffusion-controlled processes.[2,76,89] The exponent for the Gr-Chit hydrogel probed in the absence of mediators ($b = 0.96$) supports the hypothesis that electron-transfer is associated with the surface controlled double layer formation (i.e., the capacitive charge). The exponent (b) of Cat-Gr-Chit hydrogel without mediators is slightly decreased ($b = 0.82$), which might be due to the additional surface-controlled redox reaction of conducting catechol. Last, the lowest exponent for the Cat-Gr-Chit probed in the presence of mediators ($b = 0.65$) supports the hypothesis that mediator diffusion is required for electron-transfer with the non-conducting catechols (note: Figure S8, Supporting Information, provides similar analysis based on potentials of oxidative peak that further support the above mechanistic interpretation[2,88,90]).

In summary, the results of Figure 5 provide electrochemical evidence that electron flow in the Cat-Gr-Chit hydrogel in the presence of mediators involves the three mechanisms suggested in Scheme 1c.

2.4. Functional Properties

2.4.1. Stability of Redox-State Switching

Redox-active catechol-based hydrogels are being examined for biosensing and bioelectronics applications[6,62,91] because their ability to be repeatedly switched between two stable redox states confers unique molecular electronic properties (e.g., molecular memory). To examine if the incorporation of graphene into the composite effects redox-switching, we evaluated the thin films of Figure 4. First, we examined the repeatability of switching over 10 cycles using an oscillating input potential (note: Figure S9, Supporting Information, shows the time series output responses). **Figure 6**a shows that when the Cat-Gr-Chit hydrogel was probed with mediators, comparatively large amplitudes for the electrical output ($\Delta Q = 4.09$ mC $\pm$ 0.12) and optical output ($\Delta A_{480} = 0.051 \pm 0.0036$) were observed and these amplitudes remained relatively constant over 10 cycles. Similarly, steady, albeit lower, amplitude outputs were observed when the Cat-Gr-Chit hydrogel was probed without mediators. This steady output indicates that the catechol moieties (both conducting and non-conducting) can be repeatedly switched.

Next, we imposed step changes in potential between −0.6 and +0.6 V and observed the resulting response in charge (Q) and absorbance (A). Figure 6b shows a repeatable response of both these electrical and optical outputs with the amplitude of

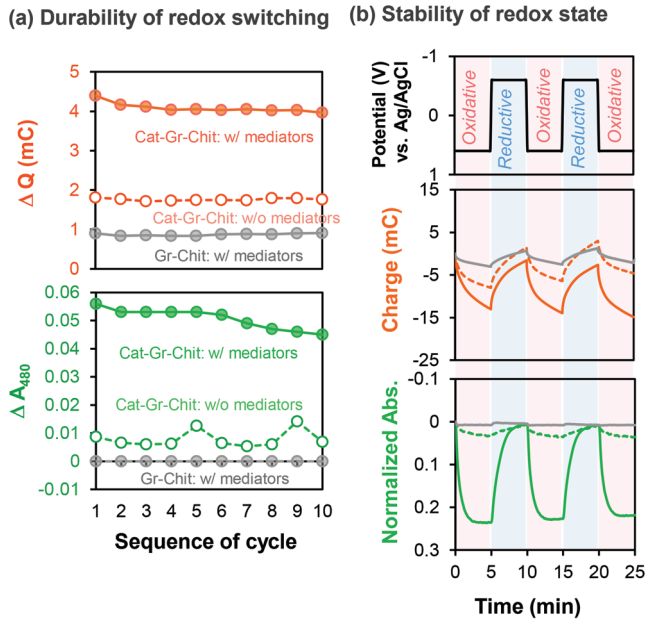

Figure 6. Stability of redox state switching. a) Repeatable switching of catechol redox-states with and without mediators as measured from the optical output from multi-cycle CV measurements (scan rate of 10 mV s^{-1}). b) Stability measurements of the reduced and oxidized redox-states of the catechol when a step potential was imposed.

the response for the Cat-Gr-Chit hydrogel being larger when the mediators were used to switch the redox-state. The absorbance plot also shows that the switched redox state remains stable when the step potential is maintained for 5 min. In subsequent studies (Figure S10, Supporting Information), we observed that these redox states were stable in the absence of sustained power for minutes to hours[6,60,63] which is comparable to stabilities reported for electrochromic materials.[2,3,16,34,36,64,92,93] Overall, the results of Figure 6 indicate that the redox-states of both the conducting and non-conducting populations of catechol can be repeatedly switched.

2.4.2. Capacitor for Charge Storage

One potential application for conducting and redox-active composite hydrogels is for energy storage. For this, we electrofabricated thick films (electrodepositing of Gr-Chit hydrogel for 5 min and catechol-grafting to a q_{Fab} of 0.96 C cm^{-2}), and generated galvanostatic charge–discharge (GCD) curves. The results of **Figure 7**a show that the charging–discharging curve for the Gr-Chit hydrogel is straight and symmetrical. Such GCD shapes have been observed for conductive materials with surface controlled EDL capacitance.[2,76] For our hydrogels, we attribute this linear-symmetric GCD behavior to the conducting graphene component in our films.

Figure 7a shows that the addition of catechol (i.e., the Cat-Gr-Chit hydrogel) broadened the GCD curve and changed the shape to have slope changes at potential values (E1 = +0.19 V and E2 = −0.16 V) that correspond to the redox potentials of the conducting catechols (observed in the CV curves of Figure 2). Such changes in slope in GCD curves have been previously observed for materials that offer a pseudo-capacitive charge-storage mechanism.[1,76] For our hydrogels, we attribute this pseudo-capacitive behavior to the conducting catechol population.

When measurements of the Cat-Gr-Chit hydrogel were performed in the presence of mediators, Figure 7a shows that the GCD results were further broadened, and partially flattened regions appeared at potential values near those observed in the CV curves of Figure 5a for the two mediators (E3 = +0.26 V and E4 = −0.29 V) (note: Figure S11, Supporting Information provides a summary of these CV and GCD results measured using the same hydrogel). Such complex shapes of the GCD curve have also been observed with battery-type materials that employ diffusion-based charge-transfer mechanisms (e.g., ion/metal intercalation).[7,94] For our hydrogels, we attribute this behavior to the non-conducting catechol population that requires mediator diffusion for charge-transfer. Overall, the shape features of the GCD curves in Figure 7a are consistent with: CV measurements in Figure S11, Supporting Information; observations for various energy storage materials;[1,2,76] and expectations for the different electron-transfer mechanisms illustrated in Scheme 1c.

While our goal was not to create a composite optimized for energy applications, it is useful to quantify the relevant energy properties of our hydrogel films. Experimentally, we calculated the specific capacity by dividing the capacity (mAh) measured from the GCD curves by the hydrogel mass and surface area as measured using a Quartz Crystal Microbalance. Figure 7b shows the calculated specific capacities of 4 different

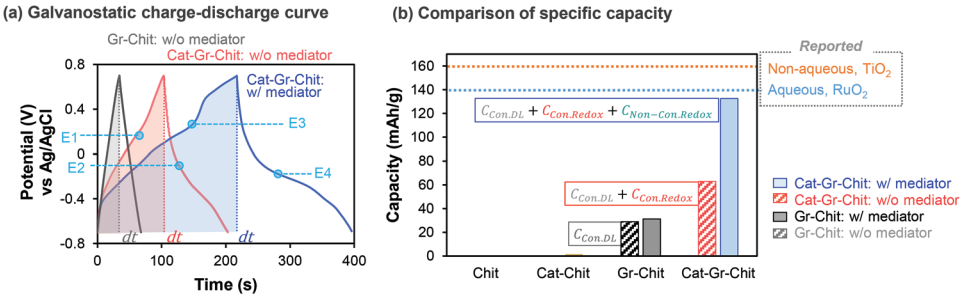

Figure 7. Catechol-based enhancement of capacitance. a) Potential outputs from galvanostatic charge–discharge (GCD) measurements at a current density of 0.63 mA cm^{-2}. b) Comparison of the specific capacities of the four hydrogels without and with mediators and also literature reports of TiO_2[2] and RuO_2[2] pseudocapacitors.

hydrogels in the buffer solution without and with mediators. First, the addition of graphene to the chitosan hydrogel significantly (≈100 times) enhanced the capacity $\left(C^{PB}_{Gr.Chit} \approx 100 C^{PB}_{Chit}\right)$ presumably due to graphene's ability to enhance the double layer capacitance. Second, the addition of catechol to the Gr-Chit hydrogel resulted in an additional 2.2-fold increase in capacity $\left(C^{PB}_{Cat.Gr.Chit} \approx 2.2 C^{PB}_{Gr.Chit}\right)$ presumably due to the addition of the conducting catechol's redox capacitance. Finally, the use of mediators yielded a further 2-fold increase in capacity $\left(C^{Mediator}_{Cat.Gr.Chit} \approx 2 C^{PB}_{Cat.Gr.Chit}\right)$ presumably due to the redox activity of the non-conducting catechols. Thus, as illustrated in Figure 7b, the capacity of our hydrogel films was synergistically increased by the addition of graphene and catechol, and the use of mediators. For comparison, Figure 7b also shows that the observed capacities of our hydrogels are ≈80% to ≈90% of the highest-reported values for energy materials in non-aqueous and aqueous systems.[2]

3. Conclusions

Here, we electrofabricated a composite hydrogel film and used a range of electrochemical methods to demonstrate that: the graphene component confers conductivity and enables charge-storage through an EDL capacitance mechanism; and the catechol component enables charge-storage through a redox mechanism. Note: Table S1, Supporting Information, provides a list of various inter-related property measurements. Further, we report two functional populations of catechol: conducting-catechols can directly transfer electrons to graphene, while non-conducting catechols require diffusible mediators for electron-transfer. The mechanistic behavior of these composite films is summarized in Figure 4e which shows the correlation between the amount of charge that can be transferred into/from the film (ΔQ) and the redox-state switching of the catechol moieties (ΔA). In the absence of catechol (i.e., the Gr-Chit hydrogel), a comparatively small amount of charge can be transferred into and out of the hydrogel through double-layer charging. The addition of catechol (i.e., the Cat-Gr-Chit hydrogel) increases charge-transfer and this increase shows a linear correlation to the molecular redox-switching of catechol moieties. The use of mediators with Cat-Gr-Chit film further enhances charge-transfer and the redox-switching of catechol by enabling electron-exchange with the non-conducting catechol population.

While the importance of conducting materials (e.g., graphene) for electronic materials is well-established, the potential benefits of redox components (e.g., catechol) are still being revealed. Using thin, partially-transparent Cat-Gr-Chit composite hydrogels, we show that the ability of catechol to exist in two stable redox states enables an optically-readable molecular-memory with switching capabilities comparable to those observed for various electrochromic materials. Using thick, Cat-Gr-Chit composite hydrogels, we show that the ability of catechol to store charge enhances capacities to values comparable to those of recently reported energy storage materials. Importantly, we demonstrate the importance of diffusible mediators to enhance the performance of redox-based energy materials.

Supporting Information

Supporting Information is available from the Wiley Online Library or from the author.

Acknowledgements

The authors acknowledge the support of the Maryland NanoCenter and its AIMLab. This work was supported by the National Science Foundation (CBET #1932963), the Defense Threat Reduction Agency (HDTRA1-19-0021), and the Department of Energy, OBER, Lawrence Livermore National Laboratory SFA (under Contract DE-AC52-07NA27344, LLNL-JRNL-827946).

Conflict of Interest

The authors declare no conflict of interest.

Data Availability Statement

The data that support the findings of this study are available in the supplementary material of this article.

Keywords

catechols, charge storage, chitosan, electrofabrication, graphene, molecular memory, redox

Received: September 12, 2022
Published online: October 20, 2022

[1] S. Fleischmann, J. B. Mitchell, R. Wang, C. Zhan, D. Jiang, V. Presser, V. Augustyn, *Chem. Rev.* **2020**, *120*, 6738.
[2] C. Choi, D. S. Ashby, D. M. Butts, R. H. DeBlock, Q. Wei, J. Lau, B. Dunn, *Nat. Rev. Mater.* **2020**, *5*, 5.
[3] L. Liu, P. L. Taberna, B. Dunn, P. Simon, *ACS Energy Lett.* **2021**, *6*, 4311.
[4] A. S. Sharova, F. Melloni, G. Lanzani, C. J. Bettinger, M. Caironi, *Adv. Mater. Technol.* **2021**, *6*, 2000757.
[5] Z. Jin, L. Yang, S. Shi, T. Wang, G. Duan, X. Liu, Y. Li, *Adv. Funct. Mater.* **2021**, *31*, 2103391.
[6] S. Wu, E. Kim, C. yu Chen, J. Li, E. VanArsdale, C. Grieco, B. Kohler, W. E. Bentley, X. Shi, G. F. Payne, *Adv. Electron. Mater.* **2020**, *6*, 2000452.
[7] B. D. Paulsen, K. Tybrandt, E. Stavrinidou, J. Rivnay, *Nat. Mater.* **2020**, *19*, 13.
[8] N. Amdursky, E. D. Głowacki, P. Meredith, *Adv. Mater.* **2019**, *31*, 1802221.
[9] J. Rivnay, S. Inal, A. Salleo, R. M. Owens, M. Berggren, G. G. Malliaras, *Nat. Rev. Mater.* **2018**, *3*, 17086.
[10] A. Sood, A. D. Poletayev, D. A. Cogswell, P. M. Csernica, J. T. Mefford, D. Fraggedakis, M. F. Toney, A. M. Lindenberg, M. Z. Bazant, W. C. Chueh, *Nat. Rev. Mater.* **2021**, *6*, 847.
[11] Z. Zhao, S. Wu, E. Kim, C. Y. Chen, J. R. Rzasa, X. Shi, W. E. Bentley, G. F. Payne, *ACS Appl. Electron. Mater.* **2022**, *4*, 2490.
[12] J. Li, Z. Zhao, E. Kim, J. R. Rzasa, G. Zong, L.-X. Wang, W. E. Bentley, G. F. Payne, *iScience* **2022**, *25*, 104548.
[13] Z. Zhao, E. E. Ozcan, E. VanArsdale, J. Li, E. Kim, A. D. Sandler, D. L. Kelly, W. E. Bentley, G. F. Payne, *ACS Chem. Biol.* **2021**, *16*, 1099.

[14] A. Ambrosi, C. K. Chua, A. Bonanni, M. Pumera, *Chem. Rev.* **2014**, *114*, 7150.
[15] X. Wang, G. Shi, *Phys. Chem. Chem. Phys.* **2015**, *17*, 28484.
[16] Q. Dou, H. S. Park, *Energy Environ. Mater.* **2020**, *3*, 286.
[17] A. Borenstein, O. Hanna, R. Attias, S. Luski, T. Brousse, D. Aurbach, *J. Mater. Chem. A* **2017**, *5*, 12653.
[18] P. Simon, Y. Gogotsi, *Nat. Mater.* **2008**, *7*, 845.
[19] E. Pomerantseva, F. Bonaccorso, X. Feng, Y. Cui, Y. Gogotsi, *Science* **2019**, *366*, 969.
[20] A. Afif, S. M. Rahman, A. Tasfiah Azad, J. Zaini, M. A. Islam, A. K. Azad, *J. Energy Storage* **2019**, *25*, 100852.
[21] Y. Wang, L. Zhang, H. Hou, W. Xu, G. Duan, S. He, K. Liu, S. Jiang, *J. Mater. Sci.* **2021**, *56*, 173.
[22] M. Kang, E. Kim, T. E. Winkler, G. Banis, Y. Liu, C. A. Kitchen, D. L. Kelly, R. Ghodssi, G. F. Payne, *Biosens. Bioelectron.* **2017**, *95*, 55.
[23] H. C. A. Murthy, K. G. Kelele, C. R. Ravikumar, H. P. Nagaswarupa, A. Tadesse, T. Desalegn, *Results Chem.* **2021**, *3*, 100131.
[24] P. Bollella, G. Fusco, C. Tortolini, G. Sanzò, G. Favero, L. Gorton, R. Antiochia, *Biosens. Bioelectron.* **2017**, *89*, 152.
[25] J. Kim, J. H. Kim, K. Ariga, *Joule* **2017**, *1*, 739.
[26] H. Li, O. Mergel, P. Jain, X. Li, H. Peng, K. Rahimi, S. Singh, F. A. Plamper, A. Pich, *Soft Matter* **2019**, *15*, 8589.
[27] C. Lu, G. Pan, Q. Huang, H. Wu, W. Sun, Z. Wang, K. Sun, *J. Mater. Chem. A* **2019**, *7*, 4438.
[28] W. Choi, S. Ohtani, K. Oyaizu, H. Nishide, K. E. Geckeler, *Adv. Mater.* **2011**, *23*, 4440.
[29] E. C. Montoto, G. Nagarjuna, J. Hui, M. Burgess, N. M. Sekerak, K. Hernández-Burgos, T. S. Wei, M. Kneer, J. Grolman, K. J. Cheng, J. A. Lewis, J. S. Moore, J. Rodríguez-López, *J. Am. Chem. Soc.* **2016**, *138*, 13230.
[30] C. Karlsson, T. Suga, H. Nishide, *ACS Appl. Mater. Interfaces* **2017**, *9*, 10692.
[31] J. Zhu, T. Zhu, H. Tuo, M. Yan, W. Zhang, G. Zhang, X. Yang, *Macromol. Chem. Phys.* **2020**, *221*, 2000160.
[32] J. K. Kim, Y. Kim, S. Park, H. Ko, Y. Kim, *Energy Environ. Sci.* **2016**, *9*, 1264.
[33] M. Burgess, K. Hernández-Burgos, J. K. Schuh, J. Davila, E. C. Montoto, R. H. Ewoldt, J. Rodríguez-López, *J. Am. Chem. Soc.* **2018**, *140*, 2093.
[34] R. Kumar, D. K. Pathak, A. Chaudhary, *J. Phys. D: Appl. Phys.* **2021**, *54*, 503002.
[35] P. M. Beaujuge, J. R. Reynolds, *Chem. Rev.* **2010**, *110*, 268.
[36] G. Yang, Y. M. Zhang, Y. Cai, B. Yang, C. Gu, S. X. A. Zhang, *Chem. Soc. Rev.* **2020**, *49*, 8687.
[37] J. T. Friedlein, R. R. McLeod, J. Rivnay, *Org. Electron.* **2018**, *63*, 398.
[38] Y. Van De Burgt, A. Melianas, S. T. Keene, G. Malliaras, A. Salleo, *Nat. Electron.* **2018**, *1*, 386.
[39] J. Li, S. P. Wang, G. Zong, E. Kim, C. Y. Tsao, E. VanArsdale, L. X. Wang, W. E. Bentley, G. F. Payne, *Adv. Mater.* **2021**, *33*, 2007758.
[40] W. Cao, A. J. Mantanona, H. Mao, N. C. McCallum, Y. Jiao, C. Battistella, V. Caponetti, N. Zang, M. P. Thompson, M. Montalti, J. F. Stoddart, M. R. Wasielewski, J. D. Rinehart, N. C. Gianneschi, *Chem. Mater.* **2020**, *32*, 5759.
[41] M. Yuan, S. D. Minteer, *Curr. Opin. Electrochem.* **2019**, *15*, 1.
[42] L. Hu, T. Zhai, H. Li, Y. Wang, *ChemSusChem* **2019**, *12*, 1118.
[43] D. Fang, G. Gao, Y. Yang, Y. Wang, L. Gao, J. Zhi, *ChemElectroChem* **2020**, *7*, 2513.
[44] C. M. Wong, C. S. Sevov, *ACS Energy Lett.* **2021**, *6*, 1271.
[45] K. Nasrin, S. Gokulnath, M. Karnan, K. Subramani, M. Sathish, *Energy Fuels* **2021**, *35*, 6465.
[46] W. Qin, N. Zhou, C. Wu, M. Xie, H. Sun, Y. Guo, L. Pan, *ACS Omega* **2020**, *5*, 3801.
[47] L. Ren, G. Zhang, Z. Yan, L. Kang, H. Xu, F. Shi, Z. Lei, Z. H. Liu, *Electrochim. Acta* **2017**, *231*, 705.
[48] M. F. Mousavi, M. Hashemi, M. S. Rahmanifar, A. Noori, *Electrochim. Acta* **2017**, *228*, 290.
[49] S. Wu, K. Yan, J. Li, R. N. Huynh, C. B. Raub, J. Shen, X. Shi, G. F. Payne, *React. Funct. Polym.* **2020**, *148*, 104492.
[50] Y. Wang, Z. Geng, M. Guo, Y. Chen, X. Guo, X. Wang, *ACS Appl. Mater. Interfaces* **2014**, *6*, 15510.
[51] E. Kim, Y. Xiong, Y. Cheng, H. C. Wu, Y. Liu, B. H. Morrow, H. Ben-Yoav, R. Ghodssi, G. W. Rubloff, J. Shen, W. E. Bentley, X. Shi, G. F. Payne, *Polymers* **2015**, *7*, 1.
[52] F. Ordikhani, M. R. Farani, M. Dehghani, E. Tamjid, A. Simchi, *Carbon* **2015**, *84*, 91.
[53] E. Avcu, F. E. Baştan, H. Z. Abdullah, M. A. U. Rehman, Y. Y. Avcu, A. R. Boccaccini, *Prog. Mater. Sci.* **2019**, *103*, 69.
[54] E. Kim, Y. Liu, W. E. Bentley, G. F. Payne, *Adv. Funct. Mater.* **2012**, *22*, 1409.
[55] J. Yang, V. Saggiomo, A. H. Velders, M. A. C. Stuart, M. Kamperman, *PLoS One* **2016**, *11*, 0166490.
[56] W. Cao, X. Zhou, N. C. McCallum, Z. Hu, Q. Z. Ni, U. Kapoor, C. M. Heil, K. S. Cay, T. Zand, A. J. Mantanona, A. Jayaraman, A. Dhinojwala, D. D. Deheyn, M. D. Shawkey, M. D. Burkart, J. D. Rinehart, N. C. Gianneschi, *J. Am. Chem. Soc.* **2021**, *143*, 2622.
[57] M. d'Ischia, A. Napolitano, A. Pezzella, P. Meredith, M. Buehler, *Angew. Chem., Int. Ed.* **2020**, *59*, 11196.
[58] T. G. Barclay, H. M. Hegab, S. R. Clarke, M. Ginic-Markovic, *Adv. Mater. Interfaces* **2017**, *4*, 1601192.
[59] J. Liebscher, *Eur. J. Org. Chem.* **2019**, *2019*, 4976.
[60] S. Wu, E. Kim, J. Li, W. E. Bentley, X. W. Shi, G. F. Payne, *ACS Appl. Electron. Mater.* **2019**, *1*, 1337.
[61] E. Kim, W. T. Leverage, Y. Liu, I. M. White, W. E. Bentley, G. F. Payne, *Analyst* **2014**, *139*, 32.
[62] E. Kim, J. Li, M. Kang, D. L. Kelly, S. Chen, A. Napolitano, L. Panzella, X. Shi, K. Yan, S. Wu, J. Shen, W. E. Bentley, G. F. Payne, *Proc. IEEE* **2019**, *107*, 1402.
[63] S. Wu, Z. Zhao, J. R. Rzasa, E. Kim, J. Li, E. VanArsdale, W. E. Bentley, X. Shi, G. F. Payne, *Adv. Funct. Mater.* **2021**, *31*, 2007709.
[64] W. Zhang, X. Wang, Y. Wang, G. Yang, C. Gu, W. Zheng, Y. M. Zhang, M. Li, S. X. A. Zhang, *Nat. Commun.* **2019**, *E10*, 1559.
[65] S. Palanisamy, B. Thirumalraj, S. M. Chen, Y. T. Wang, V. Velusamy, S. K. Ramaraj, *Sci. Rep.* **2016**, *6*, 33599.
[66] M. Forghani, S. W. Donne, *J. Electrochem. Soc.* **2018**, *165*, A664.
[67] Y. Zhou, Q. Bao, L. A. L. Tang, Y. Zhong, K. P. Loh, *Chem. Mater.* **2009**, *21*, 2950.
[68] C. Silva, F. Simon, P. Friedel, P. Pötschke, C. Zimmerer, *Nanomaterials* **2019**, *9*, 902.
[69] L. Li, Q. Liu, Y. X. Wang, H. Q. Zhao, C. S. He, H. Y. Yang, L. Gong, Y. Mu, H. Q. Yu, *Sci. Rep.* **2016**, *6*, 300082.
[70] C. Cao, E. Kim, Y. Liu, M. Kang, J. Li, J. J. Yin, H. Liu, X. Qu, C. Liu, W. E. Bentley, G. F. Payne, *Biomacromolecules* **2018**, *19*, 3502.
[71] Y. Shou, J. Zhang, S. Yan, P. Xia, P. Xu, G. Li, K. Zhang, J. Yin, *ACS Biomater. Sci. Eng.* **2020**, *6*, 3619.
[72] A. Torvi, S. Naik, M. Karidurаganavar, *Chem. Data Collect.* **2018**, *17–18*, 459.
[73] A. C. R. Fernández, N. J. Castellani, *ChemPhysChem* **2017**, *18*, 2065.
[74] Q. Wu, Y. Xu, Z. Yao, A. Liu, G. Shi, *ACS Nano* **2010**, *4*, 1963.
[75] B. A. Mei, O. Munteshari, J. Lau, B. Dunn, L. Pilon, *J. Phys. Chem. C* **2018**, *122*, 194.
[76] T. S. Mathis, N. Kurra, X. Wang, D. Pinto, P. Simon, Y. Gogotsi, *Adv. Energy Mater.* **2019**, *9*, 1902007.
[77] A. M. P. Sakita, R. D. Noce, R. L. Lavall, *J. Electrochem. Soc.* **2021**, *168*, 080525.
[78] F. Podjaski, B. V. Lotsch, *Adv. Energy Mater.* **2021**, *11*, 2003049.
[79] M. Biswal, A. Banerjee, M. Deo, S. Ogale, *Energy Environ. Sci.* **2013**, *6*, 1249.

[80] S. Roldán, C. Blanco, M. Granda, R. Menéndez, R. Santamaría, *Angew. Chem., Int. Ed.* **2011**, *50*, 1699.
[81] L. C. Almeida, R. D. Correia, A. Marta, G. Squillaci, A. Morana, F. La Cara, J. P. Correia, A. S. Viana, *Appl. Surf. Sci.* **2019**, *480*, 979.
[82] D. R. Kumar, S. Kesavan, T. T. Nguyen, J. Hwang, C. Lamiel, J. J. Shim, *Sens. Actuators, B* **2017**, *240*, 818.
[83] J. J. Han, N. Zhang, D. L. Liu, H. Ma, T. Han, D. D. Sun, *Ionics* **2020**, *26*, 1029.
[84] Y. Wang, R. Shen, S. Wang, Y. M. Zhang, S. X. A. Zhang, *Adv. Mater.* **2022**, *34*, 2104413.
[85] T. E. Winkler, H. Ben-Yoav, S. E. Chocron, E. Kim, D. L. Kelly, G. F. Payne, R. Ghodssi, *Langmuir* **2014**, *30*, 14686.
[86] E. Kim, Z. Liu, Y. Liu, W. E. Bentley, G. F. Payne, *Biomimetics* **2017**, *2*, 11.
[87] W. Y. Tsai, R. Wang, S. Boyd, V. Augustyn, N. Balke, *Nano Energy* **2021**, *81*, 105592.
[88] V. Augustyn, J. Come, M. A. Lowe, J. W. Kim, P. L. Taberna, S. H. Tolbert, H. D. Abruña, P. Simon, B. Dunn, *Nat. Mater.* **2013**, *12*, 518.
[89] M. R. Lukatskaya, S. Kota, Z. Lin, M.-Q. Zhao, N. Shpigel, M. D. Levi, J. Halim, P.-L. Taberna, M. W. Barsoum, P. Simon, Y. Gogotsi, *Nat. Energy* **2017**, *2*, 17105.
[90] C. Costentin, T. R. Porter, J. M. Savéant, *ACS Appl. Mater. Interfaces* **2017**, *9*, 8649.
[91] E. VanArsdale, J. Pitzer, G. F. Payne, W. E. Bentley, *iScience* **2020**, *23*, 101545.
[92] A. Muzaffar, M. B. Ahamed, K. Deshmukh, J. Thirumalai, *Renewable Sustainable Energy Rev.* **2019**, *101*, 123.
[93] W. Raza, F. Ali, N. Raza, Y. Luo, K. H. Kim, J. Yang, S. Kumar, A. Mehmood, E. E. Kwon, *Nano Energy* **2018**, *52*, 441.
[94] B. D. Paulsen, S. Fabiano, J. Rivnay, *Annu. Rev. Mater. Res.* **2021**, *51*, 73.